Lawrence Berkeley National Laboratory

Experimental Demonstration of Frequency Regulation – Part II: Results and Performance Evaluation

Evangelos Vrettos[1], Emre Can Kara[2], Jason MacDonald[3], Goran Andersson[1], and Duncan S. Callaway[4]

[1]Power Systems Laboratory, ETH Zurich
[2]SLAC National Accelerator Laboratory
[3]Lawrence Berkeley National Laboratory
[4]University of California, Berkeley

November 2016

Published in IEEE Transactions on Smart Grid
DOI: 10.1109/TSG.2016.2628893

Please cite as: E. Vrettos; E. C. Kara; J. MacDonald; G. Andersson; D. S. Callaway, "Experimental Demonstration of Frequency Regulation by Commercial Buildings – Part II: Results and Performance Evaluation," in *IEEE Transactions on Smart Grid* , vol.PP, no.99, pp.1-1

The work described in this study was coordinated by the Consortium for Electric Reliability Technology Solutions (CERTS), and was funded by the U.S. Department of Energy's Office of Electricity Delivery and Energy Reliability under Lawrence Berkeley National Laboratory Contract No. DE-AC02-05CH11231.

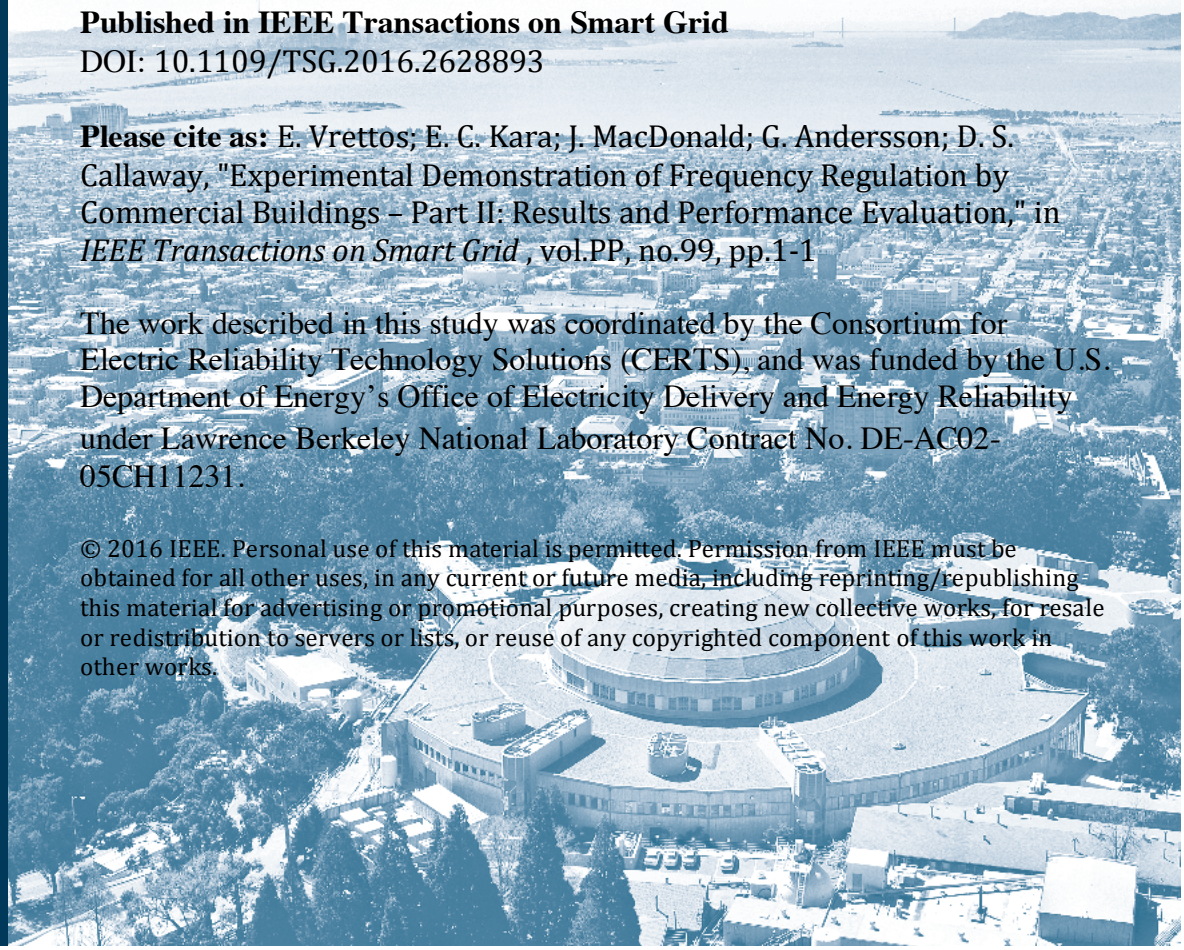

Lawrence Berkeley National Laboratory

One Cyclotron Road | Berkeley, California 94720

Prepared for the U.S. Department of Energy under Contract No. DE-AC02-05CH11231

15-PA-1015

Disclaimer

This article has been accepted for publication in a future issue of this journal, but has not been fully edited. Content may change prior to final publication. Citation information: DOI 10.1109/TSG.2016.2628893, IEEE Transactions on Smart Grid

Experimental Demonstration of Frequency Regulation by Commercial Buildings – Part II: Results and Performance Evaluation

Evangelos Vrettos, *Student Member, IEEE,* Emre C. Kara, *Member, IEEE,* Jason MacDonald, *Student Member, IEEE,* Göran Andersson, *Fellow, IEEE,* and Duncan S. Callaway, *Member, IEEE*

***Abstract*—This paper is the second part of a two-part series presenting the results from an experimental demonstration of frequency regulation in a commercial building test facility. In Part I, we developed relevant building models and designed a hierarchical controller for reserve scheduling, building climate control and frequency regulation.**

In Part II, we introduce the communication architecture and experiment settings, and present extensive experimental results under frequency regulation. More specifically, we compute the day-ahead reserve capacity of the test facility under different assumptions and conditions. Furthermore, we demonstrate the ability of model predictive control to satisfy comfort constraints under frequency regulation, and show that fan speed control can track the fast-moving RegD signal of the Pennsylvania, Jersey, and Maryland Power Market (PJM) very accurately. In addition, we discuss potential effects of frequency regulation on building operation (e.g., increase in energy consumption, oscillations in supply air temperature, and effect on chiller cycling), and provide suggestions for real-world implementation projects. Our results show that hierarchical control is appropriate for frequency regulation from commercial buildings.

***Index Terms*—ancillary services; frequency control; demand response; commercial building; HVAC system; MPC.**

I. Introduction

In Part I of this two-part paper [1], we performed a detailed literature review on theoretical, simulation-based, and experimental work on frequency regulation with the Heating, Ventilation and Air-Conditioning (HVAC) systems of commercial buildings. Furthermore, we presented the test facility for our experiment (FLEXLAB), developed relevant building models, and designed a hierarchical control scheme for provision of frequency regulation.

The scheme consists of three levels: (i) a reserve scheduler (level 1) that is formulated as a multi-period robust optimization problem; (ii) a building climate controller (level 2) that is formulated as a Model Predictive Control (MPC) problem; and (iii) a switched controller that controls fan speed in order to track a frequency regulation signal.

E. Vrettos and G. Andersson are with the Power Systems Laboratory, ETH Zurich, Switzerland, e-mails: {vrettos|andersson}@eeh.ee.ethz.ch.

E. C. Kara is with the SLAC National Accelerator Laboratory, California, US, e-mail: emrecan@slac.stanford.edu. Most of the work was carried out while E. C. Kara was at the Lawrence Berkeley National Laboratory (LBNL).

J. MacDonald is with the Grid Integration Group, LBNL, e-mail: jsmacdonald@lbl.gov.

D. S. Callaway is with the Energy and Resources Group, University of California, Berkeley, USA, e-mail: dcal@berkeley.edu.

In Section II of Part II, we summarize the control and communication architecture, as well as the experiment settings. In Sections III, IV, and V we report extensive experimental results in FLEXLAB for each level of control over a period of one week. We summarize some important findings and suggestions for future work in Section VI, whereas Section VII concludes.

II. Preparation of the Experiment

A. Communication Architecture

We implement the reserve scheduler of level 1 (solved once a day) and the MPC of level 2 (solved every 15 minutes) in Matlab, whereas we calculate the fan speed setpoints of level 3 in Python (every 4 seconds) and communicate them to the Central Working Station (CWS) of FLEXLAB. We used file-based communication between Python and Matlab based on comma-separated-values (csv) files.

The reserve scheduler stores the computed reserve capacity in a "reserve.csv" file. A Python script periodically queries the CWS and stores the building measurements in a "measure.csv" file. Another Python script periodically queries the publicly available database of forecast.io and stores the weather forecasts in a "forecast.csv" file.[1] The MPC's feedback from the building is obtained from "measure.csv" and the weather forecasts from "forecast.csv". The optimal air flow rate setpoint calculated by Matlab is stored in a "setpoint.csv" file. The fan speed setpoint is determined in Python by accessing the "setpoint.csv" and "reserve.csv" files, and based on the frequency regulation signal.

Most of the experiment was performed using archived data of the RegD signal from the Pennsylvania, Jersey, and Maryland Power Market (PJM) from December 2012 to January 2013. Although the signal was available with a resolution of 2 seconds, we down-sampled it to 4 seconds due to the expected communication delays. In addition, a connection with PJM was established based on the DNP3 protocol and using a Siemens Jetstream gateway that provided us with the RegD signal in real-time. At the FLEXLAB side, the received data were translated, saved in an SQL database, and pushed by a "RegD signal server" to a "RegD signal client". The complete communication architecture from PJM to FLEXLAB

[1]Only ambient temperature forecasts are obtained from forecast.io. The solar radiation forecasts are obtained from a clear-sky radiation model, which turned out to be sufficient for the weather conditions during the experiment.

This article has been accepted for publication in a future issue of this journal, but has not been fully edited. Content may change prior to final publication. Citation information: DOI 10.1109/TSG.2016.2628893, IEEE Transactions on Smart Grid

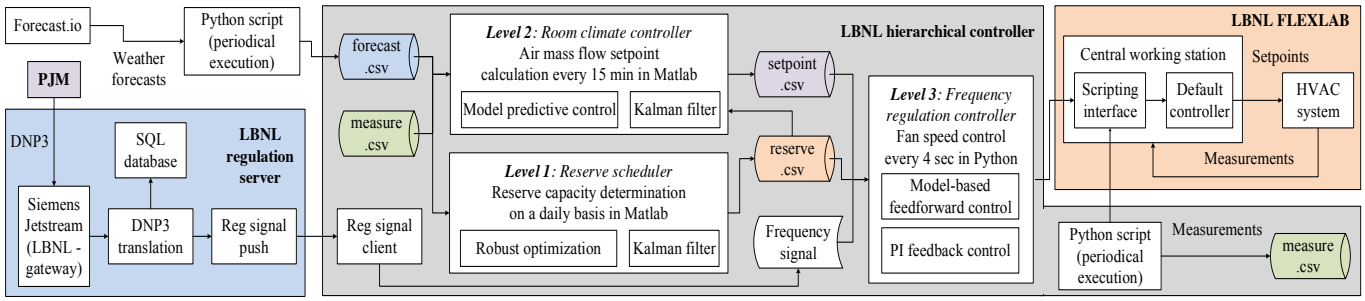

Fig. 1. The developed control and communication architecture for building climate control and frequency regulation in the FLEXLAB test facility.

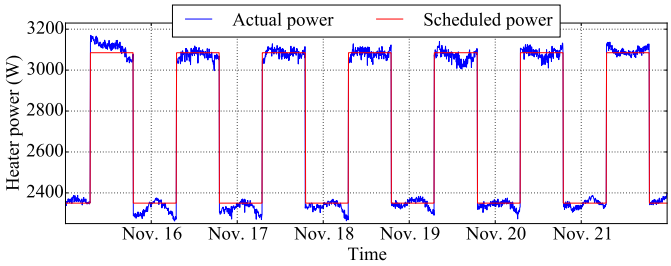

Fig. 2. The heater schedule and the actual power consumption. The heat gain is high during working hours and low during non-working hours.

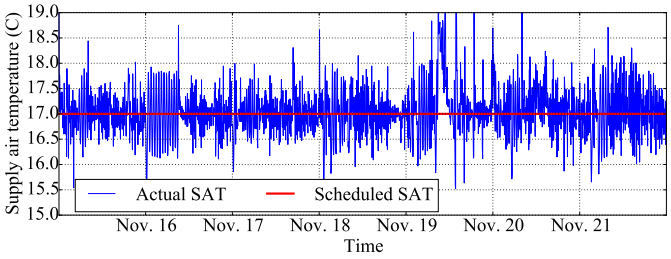

Fig. 3. The SAT setpoint and actual values during one week.

is graphically shown in Fig. 1. However, network issues at FLEXLAB made the connection unreliable, and therefore we chose to run the live connection with PJM only for one continuous hour.

B. Experiment Settings

Since FLEXLAB is not occupied, we emulated the internal heat gains from occupants and equipment using electric heaters as plug loads. The total internal heat gain in both cells was kept lower than the chiller's cooling capacity. The heaters' consumption profile was fixed according to the red curve of Fig. 2 using digital timer sockets. The actual heater power (blue curve) fluctuates around this profile due to voltage variations.

Before the start of the experiment, we fixed the manually controlled inlet dampers in the rooms to fully open positions. In addition, we fixed the return air damper to a 100% opening and the outside air damper to a 0% opening, i.e., the return air was fully recirculated. The speeds of primary and secondary chilled water pumps were fixed to 75% and 100% of their rated speeds, respectively. Moreover, we deactivated FLEXLAB's floor heating system and the heating coil at the Air Handling Unit (AHU).

We set the temperature comfort zone to $21 - 25°$C during working hours. An existing Proportional-Integral (PI) controller regulates the Supply Air Temperature (SAT) to $17°$C by controlling the position of a cooling valve. The gains of this controller had been tuned for a conventional building operation; therefore, we modified them to achieve a tighter control and reduce the fluctuations of SAT around its setpoint during frequency regulation. The resulting SAT profile during the experiment is shown in Fig. 3. The mean deviation from the SAT setpoint is $0.05°$C (there is a small bias to larger SAT values) and the mean absolute deviation is $0.37°$C.

Recall that the facility has two building cells with identical construction: cell 1A is used for the frequency regulation experiment, whereas cell 1B serves as a benchmark. Applying the same air flow rate in both cells and recording the temperature, we verified that the two cells are thermally very similar. However, we observed that the same fan speed setpoint induces a slightly different air flow rate in the two cells due to small differences in the AHUs. To compensate for this, we fitted different fan models for the two cells (the parameters for cell 1A are given in [1, Table IV]).

The electricity cost was assumed equal to $c_k = 0.18$ €/kWh, whereas the reserve capacity payment was fixed to a 10% higher value, i.e., $\lambda_k = 0.198$ €/kWh. The goal of this experiment is to demonstrate the technical feasibility of frequency regulation from commercial buildings. For this reason, we chose a relatively high capacity payment to incentivize reserve provision from FLEXLAB.

C. Experiment Plan

The experiment was organized into two parts. The first part took place from 15 to 18 November 2015 and relied on an "older" building model identified with data from June-July 2015 (see [1, Table II]). On 19 November the experiment was paused and a new building model was identified using the recently collected data (see [1, Table III]), which was used in the second part of the experiment from 20 to 21 November. Both models are identified using the "1-day ahead prediction" approach introduced in [1, Section III.A].

This article has been accepted for publication in a future issue of this journal, but has not been fully edited. Content may change prior to final publication. Citation information: DOI 10.1109/TSG.2016.2628893, IEEE Transactions on Smart Grid

III. Reserve Scheduling (Level 1)

In this section, we present results relevant to the reserve scheduler. Two main factors that determine the amount of reserves are the building's energy capacity and the symmetry of reserve capacity. Apart from the physical properties of the building, the energy capacity depends also on the comfort zone's width. In this experiment, we specifically address the effect of enlarging the comfort zone during unoccupied hours to $12-35^{\circ}$C (the so-called night setback). We performed six full-day experiments with symmetric (equal up- and down-reserves) or asymmetric reserves, and with or without night setback. Note that the same price is assumed for up- and down-reserves in the asymmetric case.

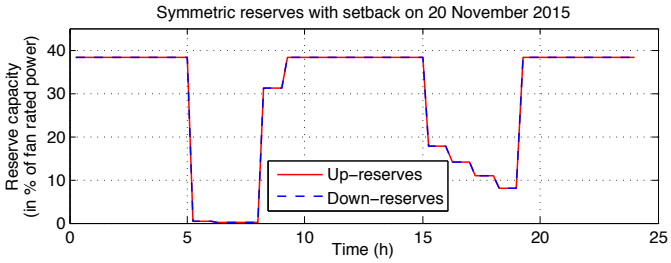

Fig. 4. The hourly, symmetric reserve capacities as a percentage of nominal fan power for 20 November 2015.

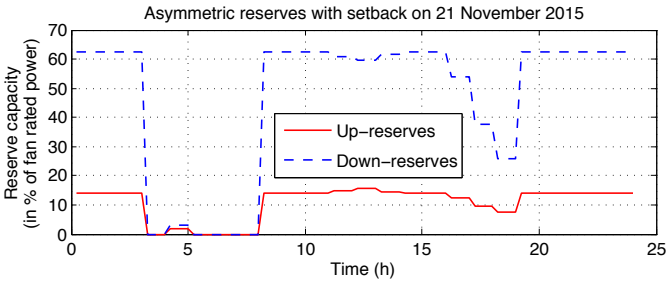

Fig. 5. The hourly, asymmetric reserve capacities as a percentage of nominal fan power for 21 November 2015.

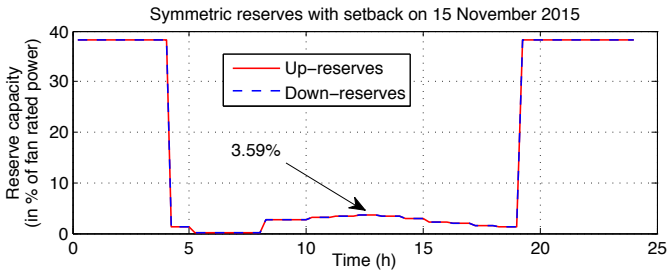

Fig. 6. The hourly, symmetric reserve capacities as a percentage of nominal fan power for 15 November 2015 (with setback).

Figure 4 shows results for 20 November when symmetric reserve capacities were assumed, and Fig. 5 for 21 November when asymmetric capacities were used (in both days night setback was applied). The capacities are reported in % of the fan rated power (2500 W). The reserve capacity is maximized at night when the comfort zone is enlarged, and during the hottest part of daytime. For symmetric reserves, the maximum capacity is slightly less than 40% of the rated fan power. For asymmetric reserves, the maximum up-reserve capacity is approximately 15%, whereas the down-reserve capacity is more than 60%. These experimental results are in agreement with relevant simulation results in [2], [3], and show that down-reserves (increase of HVAC power) are preferable for commercial buildings equipped with energy-efficient controllers, because down-reserves can be provided without increasing the baseline consumption and the energy cost.

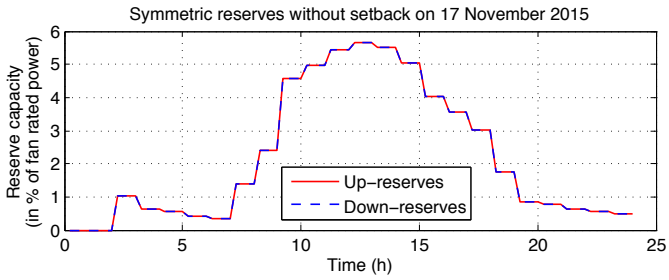

Fig. 7. The hourly, symmetric reserve capacities as a percentage of nominal fan power for 17 November 2015 (without setback).

TABLE I
Experimental (bold) and simulated (normal font) daily average reserve capacities in % of fan nominal power (2500 W).

Date	Symmetric, Setback		Asymmetric, Setback		Symmetric, No setback		Asymmetric, No setback	
	R_u	R_d	R_u	R_d	R_u	R_d	R_u	R_d
15/11	**15.61**	**15.61**	6.45	26.15	1.91	1.91	1.64	4.42
16/11	9.09	9.09	**3.90**	**14.88**	0.74	0.74	0.90	1.85
17/11	11.44	11.44	5.39	21.21	**2.24**	**2.24**	1.85	4.59
18/11	16.70	16.70	7.78	31.75	3.94	3.94	**3.28**	**9.91**
20/11	**28.95**	**28.95**	11.89	49.66	15.07	15.07	7.82	28.81
21/11	22.10	22.10	**10.72**	**46.55**	13.60	13.60	6.79	26.30

Figure 6 shows experimental results for 15 November when setback was used, whereas Fig. 7 shows results for 17 November when no setback was applied (the reserve capacities were symmetric in both dates). With setback most reserve is provided at night, whereas without setback the reserve provision coincides with the highest cooling load in the middle of the day. Although the experiment was conducted with setback and symmetric reserves both on 15 and 20 November, the capacity profiles during daytime are considerably different due to different weather conditions and building models.

To have a fair comparison under the same external conditions, we simulated the reserve capacity scheduling for all combinations of reserve symmetry and night setback using the building model. The simulation and experimental results are shown in Table I. The capacity ranges from low values below 1% to high values nearly 50%, and it heavily depends on reserve symmetry, setback, and weather conditions. The night setback increases the capacity by 177.0% on average for symmetric reserves, by 107.0% for asymmetric up-reserves, and by 150.7% for asymmetric down-reserves. If setback is already used, adopting asymmetric capacities instead of symmetric capacities reduces the up-reserves by 55.6% but increases the down-reserves by 83.1%, and so the net effect is an increase of 13.7% in the total capacity.

This article has been accepted for publication in a future issue of this journal, but has not been fully edited. Content may change prior to final publication. Citation information: DOI 10.1109/TSG.2016.2628893, IEEE Transactions on Smart Grid

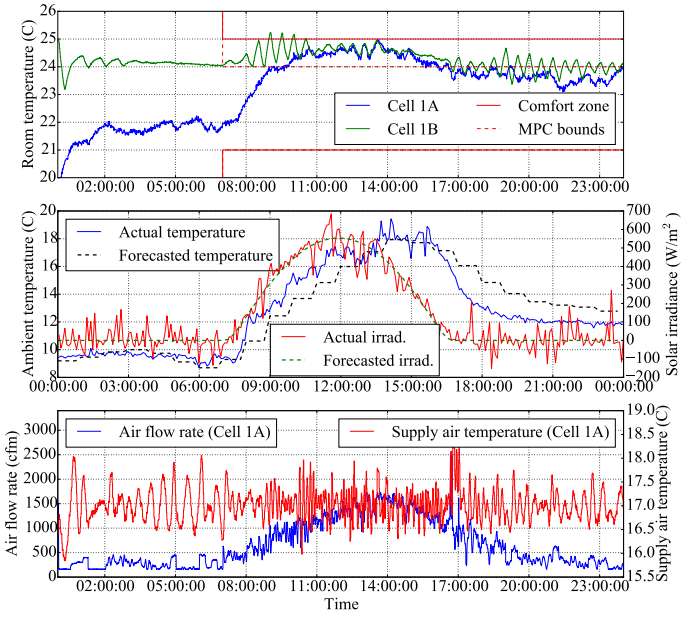

Fig. 8. Experimental results for the room climate controller under frequency regulation on 17 November (symmetric reserves, without night setback).

IV. Room Climate Control (Level 2)

A. Comfort Satisfaction

Experimental results for 17 November are shown in Fig. 8, where the top plot shows the temperature trajectories in cells 1A and 1B, the middle plot presents the forecasts and actual values for ambient temperature and solar irradiance[2], whereas the bottom plot shows the SAT and the air flow rate in cell 1A.[3] The comfort zone is indicated with red: the actual upper limit (red solid line) is 25°C, but a tighter limit of 24°C (red dashed line) is used within the MPC to account for modeling and forecast errors. Similar results for 18, 20, and 21 November are shown in Figs. 9, 10, and 11, but without including the SAT and air flow rate plots due to space limitations.

In Figures 8 and 9 the cell 1B is under energy efficient operation and the temperature remains close to the upper limit of the comfort zone. On the other hand, in Figs. 10 and 11 the cell 1B is in a "regulation-ready" operation mode, namely the consumption of the HVAC system is scheduled identically to cell 1A to allow reserve provision, but no regulation signal is received. For this reason, the temperature trajectories of the two cells are very close to each other for most of the time on 20 and 21 November.[4]

[2]The total global irradiance is shown, which includes the long-wave radiation losses from the building envelope to the atmosphere, and it can be negative at night. This effect is known as nighttime radiation cooling [4].

[3]Despite the relatively low ambient temperature during the experiment, cooling is needed due to the high internal and solar irradiance heat gains. The cooling energy is provided by the HVAC system rather than natural ventilation in order to emulate hotter days with higher reserve potential.

[4]The discrepancies from 12.00 to 19.00 on 20 November are due to the calibration differences between the fan models of the two cells (see Section II-B). The discrepancies from 07.00 to 17.00 on 21 November are because of interruptions in the hierarchical control in cell 1B due to server connection timeout error from approximately 07.00 to 11.00. When the server was unresponsive, the cell was controlled by an existing fallback controller.

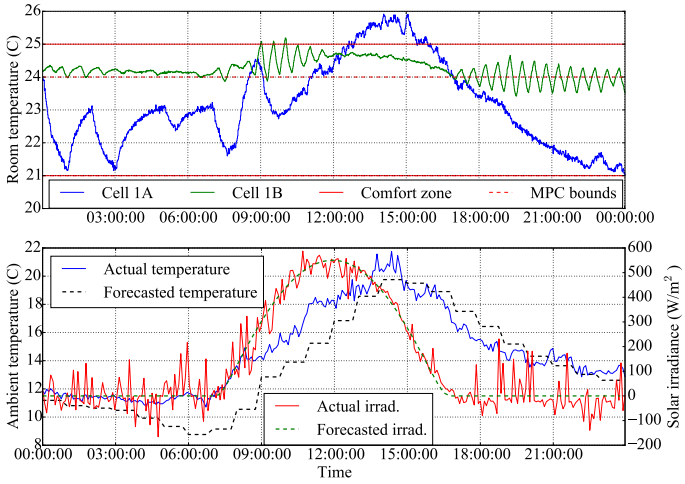

Fig. 9. Experimental results for the room climate controller under frequency regulation on 18 November (asymmetric reserves, without night setback).

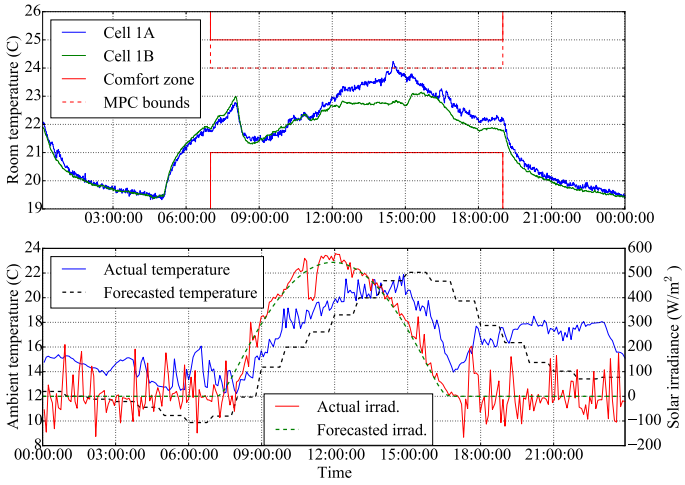

Fig. 10. Experimental results for the room climate controller under frequency regulation on 20 November (symmetric reserves, with night setback).

The temperature trajectory of cell 1B in Figs. 8 and 9 remains mostly in the band $[24-25]$°C, which illustrates the necessity of tightening the comfort zone constraints in the MPC to compensate for modeling errors. The temperature trajectory of cell 1A is more variable and it follows the scheduled reserve and air flow rate. On 17 November (Fig. 8) frequency regulation is provided while respecting the comfort zone.

However, on 18 November (Fig. 9) the comfort zone is violated from 13.00 to 16.00 in cell 1A, but not in cell 1B. This happens because: (i) the ambient temperature is higher than the day-ahead forecast from the beginning of the day until 15.00, and (ii) asymmetric reserves are used. The asymmetry allows for a more aggressive scheduling with a larger down-reserve capacity on 18 November, in comparison with 17 November when symmetric reserves are used (see Table I).

The control performance is significantly better on 20 and 21 November (Figs. 10 and 11) despite the large discrepancies between the day-ahead ambient temperature forecasts and

This article has been accepted for publication in a future issue of this journal, but has not been fully edited. Content may change prior to final publication. Citation information: DOI 10.1109/TSG.2016.2628893, IEEE Transactions on Smart Grid

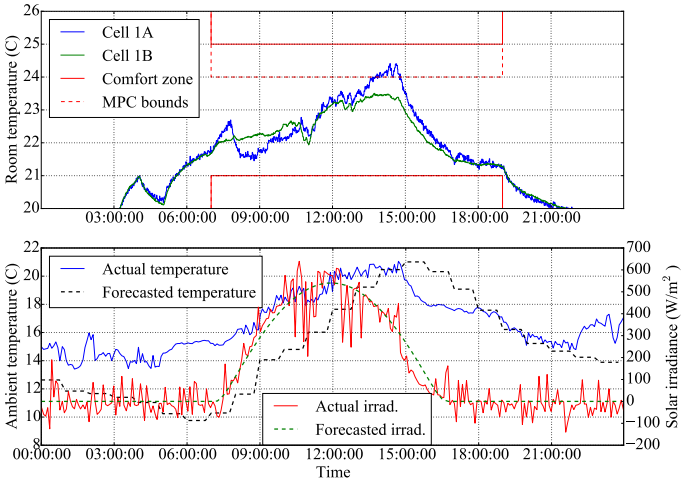

Fig. 11. Experimental results for the room climate controller under frequency regulation on 21 November (asymmetric reserves, with night setback).

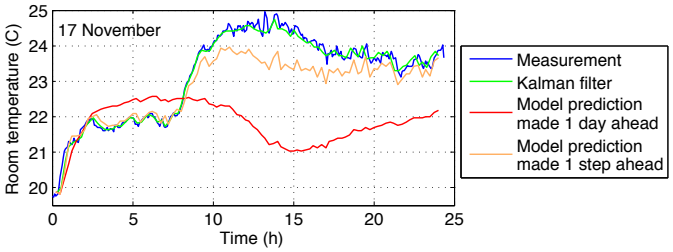

Fig. 12. Model and Kalman filter performance for 17 November, when the older building model was used.

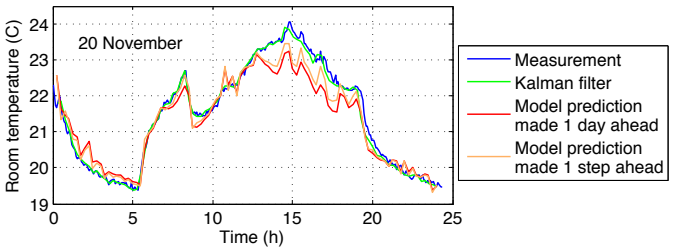

Fig. 13. Model and Kalman filter performance for 20 November, when the new building model was used.

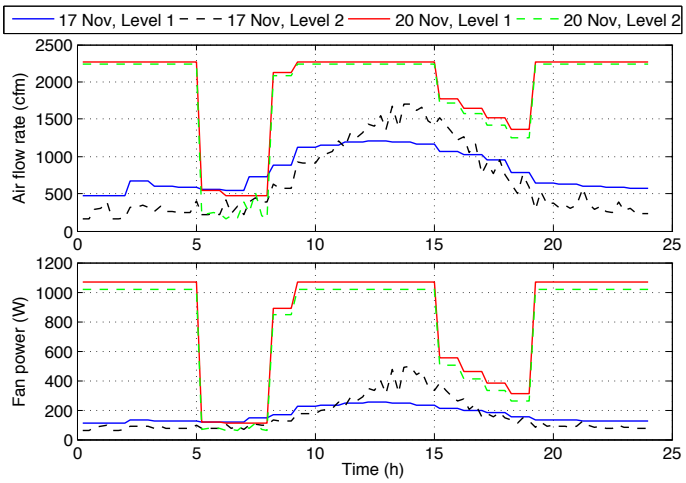

Fig. 14. Left: Air flow rate schedule in level 1 and level 2. Right: Fan power schedule in level 1 and level 2.

the actual values. The improvement is due to the recently calibrated building model (see Section II-C). No comfort zone violations occur and moreover the temperature is below the MPC constraint of 24°C for most of the time. Therefore, periodic model calibration (for example on a weekly or daily basis) is important to account for seasonality and eliminate systematic errors.

These results show that if the model and weather forecasts are sufficiently accurate, the robust reserve scheduler allows a commercial building to bid in day-ahead markets for frequency regulation. On the other hand, if the modeling and forecast errors exceed the controller's robustness margin, reserve provision for frequency regulation might have an adverse effect on occupant comfort.

The temperature trajectory in Figs. 10 and 11 is typical for a building with night setback. The controller chooses to overcool the space at night in order to generate higher revenue by offering a larger reserve capacity. In contrast, the reserve capacity is smaller during working hours and the room temperature is higher. A comparison of the temperature trajectories in cells 1A and 1B shows that tracking the RegD signal has little effect on room temperature due to the signal's limited energy content.

B. Model and Estimator Performance

Figure 12 shows the out-of-sample performance of the older model, whereas Fig. 13 shows the same results for the new model. The blue curve is the measured room temperature, and the green curve is the estimated temperature with the Kalman filter. The red curve corresponds to a temperature prediction made by the model one day ahead, whereas the orange curve shows a temperature prediction made by the model one step ahead.[5] Clearly, the new model outperforms the older one, especially for the day-ahead predictions. This is why the performance of the level 2 controller is much better on 20 November than on 17 November in terms of comfort zone violations.

The effect of model accuracy on MPC operation is shown in Fig. 14. On 17 November the model mismatch is large, which results in a significant discrepancy in the scheduled air flow rate and fan power between level 1 and level 2. The MPC reacts on the modeling error by reducing the cooling power in level 2 during night hours and increasing it during daytime. In this way, the MPC provides the same amount of electric reserve in daytime with less change in air flow rate by taking advantage of the nonlinear fan curve. On the other hand, the model mismatch is small on 20 November, and therefore the air flow and fan power schedules of level 1 and level 2 are similar. In fact, level 2 consistently schedules less cooling power than level 1 because the air flow constraints are relaxed [1, Equations 15, 24], and the reserve scheduling in level 1 is robust and thus conservative.

[5]Both the step-ahead and day-ahead predictions are generated using a model identified with the "1-day ahead prediction" approach [1, Section III.A].

This article has been accepted for publication in a future issue of this journal, but has not been fully edited. Content may change prior to final publication. Citation information: DOI 10.1109/TSG.2016.2628893, IEEE Transactions on Smart Grid

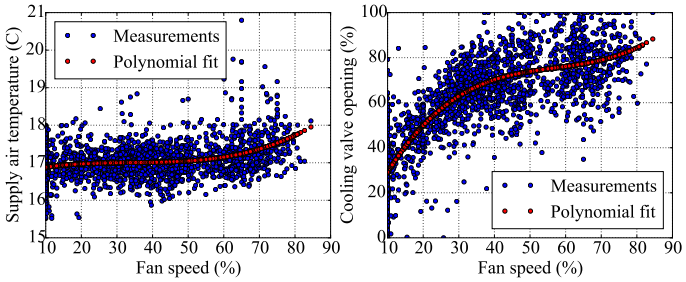

Fig. 15. The dependence of SAT and cooling valve opening on fan speed.

C. Fan Heat Gain at High Speeds

We present results on the dependence of SAT and cooling valve opening on fan speed in Fig. 15, where the blue points are measurements and the red trend is a polynomial fit on them. As expected, the trend in cooling valve opening is increasing because the higher the fan speed the more cooling is required from the chilled water loop. The trend in SAT is a flat line for fan speeds up to 50%. However, for speeds above 50% (and especially above 70%) there is a clear increasing SAT trend despite the increased cooling valve opening.

These results lead to an interesting observation: the heat gain due to fan rotation is significant at high speeds and it cannot be effectively rejected by exchanging heat with the chilled water loop. According to Fig. 15, if the fan operates at a 70% speed or higher, the SAT will likely have a steady-state deviation from the setpoint $17°$C that can be as high as $1°$C. Steady-state SAT deviations might result in comfort zone violations, because the controller assumes the SAT fixed to $17°$C. This did not create problems in our experiment because the scheduled fan speed by the MPC was at most 70%.

D. Effect on Energy Consumption

A major concern when providing Ancillary Services (AS) with commercial buildings is the effect on energy consumption. Reference [5] reported a round-trip efficiency of 46% when a building responded to demand response events in an experiment. There are two types of efficiency losses relevant to frequency regulation: "reserve availability efficiency loss" and "reserve utilization efficiency loss" [6].

The "reserve availability efficiency loss" is the efficiency loss due to scheduling the consumption in an energy suboptimal way to be able to provide frequency reserves, if requested. The reserve scheduler identifies the optimal tradeoff between minimizing energy consumption and leaving enough slack for reserve provision. Note that depending on energy and reserve prices, the building may or may not be willing to provide frequency regulation. The "reserve utilization efficiency loss" is an additional efficiency loss while tracking the frequency regulation signal.

We report efficiency results in Table II for: (i) 15-18 November when the cell 1B was under energy efficient operation (to quantify the "reserve availability efficiency loss"); and (ii) 20 November when cell 1B was in regulation-ready operation mode (to quantify the "reserve utilization efficiency loss").

TABLE II
EFFECT OF FREQUENCY REGULATION ON ENERGY CONSUMPTION

1B operation mode	Energy efficient 15/11-18/11		Regulation-ready 20/11 (0-24 h)		20/11 (0-12 h)	
Cell	1A	1B	1A	1B	1A	1B
Fan energy (kWh)	27.22	16.23	19.24	20.91	9.40	10.19
Cooling (gpm · F)	1989.92	1800.55	772.16	788.69	328.78	331.09
Mean temp. (°C)	22.85	24.43	21.45	21.26	21.05	21.05

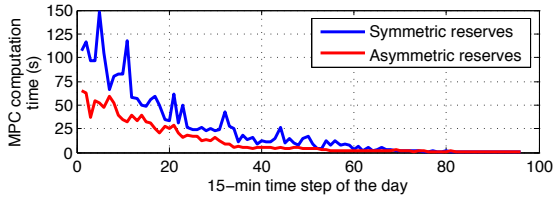

Fig. 16. The average MPC computation time depending on the time of the day and on reserve symmetry.

The efficiency loss is calculated comparing the energy consumption of cell 1A with that of the benchmark cell 1B. We use two different definitions of energy consumption: (i) electric energy consumption of the fan, and (ii) thermal cooling power consumption of each cell. The latter is calculated based on the chilled water flow rate ($\dot{m}_{\text{cw}}$), as well as the supply ($T_{\text{ch,s}}$) and return ($T_{\text{ch,r}}$) chilled water temperatures using

$$P_{\text{cool}} = \dot{m}_{\text{cw}} \cdot (T_{\text{ch,r}} - T_{\text{ch,s}}) \ . \tag{1}$$

Based on the results of Table II, the "reserve availability efficiency loss" is significant and equal to approximately 68% in terms of fan energy and 11% in terms of cooling power from the chiller. However, the additional consumption in cell 1A is not entirely wasted because it results in a lower average temperature. When cell 1B is in the regulation-ready mode, the cell 1A consumes less energy than cell 1B despite frequency regulation. The non-negligible difference in the average temperature of the two cells is due to imperfections in fan model calibration and limited temperature sensor accuracy. However, even from 00.00 to 12.00 when both average cell temperatures are $21.05°$C, the consumption of cell 1A is still lower than that of cell 1B. This result indicates that the "reserve utilization efficiency loss" is negligible while tracking a fast-moving regulation signal like RegD.

E. MPC Computation Time

The MPC computation time is sufficiently low for our demonstration. As shown in Fig. 16, the longest computation time is 150 seconds for symmetric reserves and 65 seconds for asymmetric reserves. The computation time for asymmetric reserves is lower because the problem is simpler and smaller [1, Section IV.D].

The computation time decreases at the end of the day because a reducing MPC horizon is used. After the 70^{th} time step, when the MPC prediction horizon is smaller than 26 time steps (6.5 hours), the computation time is less than 2 seconds. Therefore, Fig. 16 can be used to select the prediction horizon's length depending on the maximum

This article has been accepted for publication in a future issue of this journal, but has not been fully edited. Content may change prior to final publication. Citation information: DOI 10.1109/TSG.2016.2628893, IEEE Transactions on Smart Grid

allowable computation time. Since the computation time grows exponentially with the number of variables of the nonlinear optimization problem, a shorter prediction horizon might be necessary for larger buildings.

V. Regulation Signal Tracking (Level 3)

A. Control Performance Metrics

In this section, we present results from level 3 and evaluate the tracking performance of the regulation signal. The following metrics are used

$$e_{\mathrm{t},k} = e_{\mathrm{c},k}/P_{\mathrm{d},k}, \quad e_{\mathrm{c},k} = P_{\mathrm{d},k} - P_{\mathrm{f},k} \tag{2}$$

$$e_{\mathrm{r},k} = \begin{cases} e_{\mathrm{c},k}/R_{\mathrm{u},k}, & \text{if } w_k < 0 \\ e_{\mathrm{c},k}/R_{\mathrm{d},k}, & \text{if } w_k \geq 0 \end{cases} \tag{3}$$

$$e_{\mathrm{me}} = (1/N_{\mathrm{exp}}) \cdot \sum\nolimits_{k=0}^{N_{\mathrm{exp}}-1} e_{\mathrm{c},k} \tag{4}$$

$$e_{\mathrm{mae}} = (1/N_{\mathrm{exp}}) \cdot \sum\nolimits_{k=0}^{N_{\mathrm{exp}}-1} \left| e_{\mathrm{c},k} \right| \tag{5}$$

$$e_{\mathrm{rmse}} = \sqrt{(1/N_{\mathrm{exp}}) \cdot \sum\nolimits_{k=0}^{N_{\mathrm{exp}}-1} e_{\mathrm{c},k}^2} \tag{6}$$

$$e_{\mathrm{t,mape}} = (1/N_{\mathrm{exp}}) \cdot \sum\nolimits_{k=0}^{N_{\mathrm{exp}}-1} \left| e_{\mathrm{t},k} \right| \tag{7}$$

$$e_{\mathrm{r,mape}} = (1/N_{\mathrm{exp}}) \cdot \sum\nolimits_{k=0}^{N_{\mathrm{exp}}-1} \left| e_{\mathrm{r},k} \right| \ , \tag{8}$$

where $P_{\mathrm{f},k}$ denotes the instantaneous fan power, w_k denotes the normalized regulation signal, and N_{exp} denotes the experiment duration. The metrics $e_{\mathrm{t},k}$ and $e_{\mathrm{r},k}$ are relative instantaneous errors but the normalization is performed using the desired fan power $P_{\mathrm{d},k}$ in $e_{\mathrm{t},k}$, and the up- ($R_{\mathrm{u},k}$) or down-reserve capacity ($R_{\mathrm{d},k}$) in $e_{\mathrm{r},k}$. The mean error e_{me} is used to measure any biases in the control response, whereas e_{mae} is the Mean Absolute Error (MAE) during the experiment. The Root Mean Squared Error (RMSE) e_{rmse} penalizes more large control errors, for example due to overshoots and undershoots. The metric $e_{\mathrm{t,mape}}$ is the tracking Mean Absolute Percentage Error (MAPE), and $e_{\mathrm{r,mape}}$ is the reserve MAPE. We use the metric $e_{\mathrm{r,mape}}$ because it describes the relative size of control error with respect to reserve capacity.

In addition, we use the score proposed by PJM for evaluating the performance of frequency regulation. The total score S_{tot} consists of three parts, namely the correlation score S_{c}, the delay score S_{d} and the precision score S_{p}. The scores are computed separately for each hour according to [7]

$$S_{\mathrm{c}} = \max_{\tau \in [0,5 \text{ min}]} (R_{\mathrm{cor}}) \tag{9}$$

$$R_{\mathrm{cor}} = \frac{1}{n-1} \cdot \sum_{k=1}^{n} \left(\frac{P_{\mathrm{d},k} - \bar{P}_{\mathrm{d,h}}}{s_{\mathrm{d}}} \right) \cdot \left(\frac{P_{\mathrm{f},k} - \bar{P}_{\mathrm{f,h}}}{s_{\mathrm{f}}} \right) \tag{10}$$

$$S_{\mathrm{d}} = \left| \frac{\tau^* - 5 \text{ min}}{5 \text{ min}} \right|, \ \tau^* = \operatorname*{argmax}_{\tau \in [0,5 \text{ min}]} (R_{\mathrm{cor}}) \tag{11}$$

$$S_{\mathrm{p}} = 1 - (1/n) \cdot \sum\nolimits_{k=1}^{n} \left| \frac{e_{\mathrm{c},k}}{\bar{P}_{\mathrm{d,h}}} \right| \tag{12}$$

$$S_{\mathrm{tot}} = (1/3) \cdot S_{\mathrm{c}} + (1/3) \cdot S_{\mathrm{d}} + (1/3) \cdot S_{\mathrm{p}} \ , \tag{13}$$

where n is the number of time steps within an hour, R_{cor} is the Pearson product-moment correlation coefficient, $\bar{P}_{\mathrm{d,h}}$ (resp. $\bar{P}_{\mathrm{f,h}}$) is the hourly average value of the reference power (resp. of the actual fan power), and s_{d} (resp. s_{f}) is the standard deviation of $P_{\mathrm{d},k}$ (resp. of $P_{\mathrm{f},k}$).

The correlation score is the maximum correlation coefficient between $P_{\mathrm{d},k}$ and $P_{\mathrm{f},k}$, and τ^* is the time shift at which the correlation is maximized (τ takes a value from 0 to 5 minutes with a step of 10 seconds). We calculate the delay score based on the time shift with maximum correlation. In the precision score calculation, we normalize the absolute control error by $\bar{P}_{\mathrm{d,h}}$, whereas the total score is a weighted sum of the individual scores.

B. Experimental Time Series Results

In Fig. 17 we present results from the operation of level 3 controller from 18.30 to 19:30 on 20 November 2015. The duct pressure is quadratic to fan speed, as expected from the fan laws. Since the duct system is designed to sustain the pressure corresponding to maximum fan speed, and because the fan speed does not exceed its maximum value (90%) during frequency regulation, pressure constraints were not necessary in the reserve scheduling and MPC formulations in our experiment.

The switched controller of level 3 consists of a PI controller and a model-based feedforward controller. The RegD signal changes direction very often and has a limited energy content. During periods of time when the RegD signal is relatively flat, or the reserve capacity is low, the PI controller is active. On the other hand, whenever the changes in fan power are rapid, the control switches to the feedforward control.[6]

The tracking of the RegD signal is generally very good. However, when large rapid changes in fan power are requested, overshoots or undershoots might appear. In addition, if the reserve capacities change significantly at the beginning of each full hour, temporarily large errors might occur. In general, the instantaneous percentage errors $e_{\mathrm{t},k}$ and $e_{\mathrm{r},k}$ are higher at low operating fan power and low reserve capacity.

C. Evaluation of Tracking Performance

The performance metrics (2)-(8) for the 6 days of Table I are presented in Table III. The error metric $e_{\mathrm{r,mape}}$ is larger than $e_{\mathrm{t,mape}}$ because small reserve capacities are offered for a large part of the experiment. The mean error e_{me} has a negative bias, which means that the fan power is more often higher than the desired setpoint because the control overshoots are larger than the undershoots.

We investigate the dependence of control performance on the minimum reserve capacity, which we call "reserve threshold" and denote by R_{thr}. The metrics e_{mae}, e_{rmse}, $e_{\mathrm{t,mape}}$ and $e_{\mathrm{r,mape}}$ are recalculated considering only the time steps when $R_{\mathrm{u},k} \geq R_{\mathrm{thr}}$ if $w_k < 0$, and $R_{\mathrm{d},k} \geq R_{\mathrm{thr}}$ if $w_k \geq 0$. We repeat

[6] In principle, fast changes in fan speed increase the stress on the fan and, possibly, the device wear. However, the fan's Variable Frequency Drive (VFD) is programmed to limit the speed changes such that the fan ramps from zero to full speed no faster than 30 seconds. For this reason, we believe that the additional wear of the fan will be rather limited, and will not hinder the long-term applicability of the approach. A detailed investigation of fan's wear was not possible in this paper due to lack of relevant measurements, but it is an interesting topic of follow-up work.

This article has been accepted for publication in a future issue of this journal, but has not been fully edited. Content may change prior to final publication. Citation information: DOI 10.1109/TSG.2016.2628893, IEEE Transactions on Smart Grid

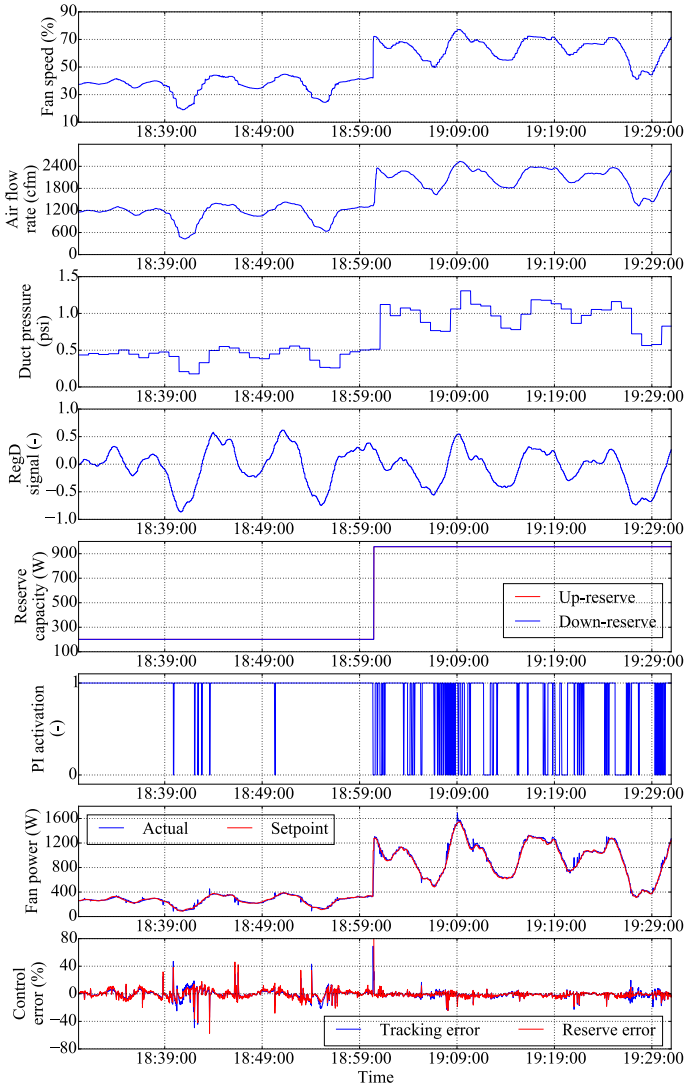

Fig. 17. Fan control and RegD signal tracking for a period of 1 hour.

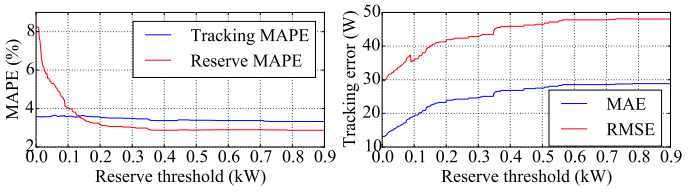

Fig. 18. Dependence of tracking and reserve errors on reserve threshold.

this procedure for different R_{thr} values and present the results in Fig. 18.

In contrast to $e_{\text{t,mape}}$, the error metric $e_{\text{r,mape}}$ decreases rapidly as R_{thr} increases in the range $[0, 200]$ W. This happens because (for the same absolute control error) $e_{\text{r},k}$ decreases if $R_{\text{u},k}$ or $R_{\text{d},k}$ increase. On the other hand, e_{mae} and e_{rmse} generally increase as R_{thr} increases because the higher the reserve capacity the larger the fan power change, and thus the higher the errors due to overshoots and undershoots. Fig. 18 can provide us with bounds on reserve capacity from a tracking performance point of view.

TABLE III
REGD TRACKING PERFORMANCE METRICS DURING THE EXPERIMENT

Metric	e_{me}	e_{mae}	e_{rmse}	$e_{\text{t,mape}}$	$e_{\text{r,mape}}$
Value	-5.66 W	12.45 W	27.00 W	3.58%	8.23%

TABLE IV
PJM SCORES FOR TRACKING THE REGD SIGNAL

Score	S_{c}	S_{d}	S_{p}	S_{tot}
$15-18$ Nov.	0.89	0.97	0.96	0.94
$20-21$ Nov.	0.96	0.99	0.98	0.98

In Table IV we report the PJM scores calculated separately for the period 15 - 18 November and the period 20 - 21 November. Different scores are calculated for each hour (only if the reserve capacity is non-zero) [7], and the values in Table IV are hourly averages. The frequency regulation performance is exceptional during the whole experiment. The scores are slightly higher for $20-21$ November because the building provides a larger reserve capacity compared with $15-18$ November.

For comparison, the highest possible total score is $S_{\text{tot}} = 1$ and the minimum S_{tot} accepted by PJM is 0.75. In the experiment reported in [8], a total score of 0.83 was achieved while tracking a RegD signal from PJM using a lag compensator (very similar to a standard PI controller). In our experiment the total performance score is significantly higher (in the range $0.94-0.98$), mainly because we use the switched controller proposed in Part I of this two-part paper [1, Section VI].

D. Effect on Supply Air Temperature

Tracking the fast-moving RegD signal introduces high frequency oscillations on SAT as shown in Fig. 19. The SAT of cell 1A (frequency regulation mode) oscillates more than that of cell 1B (regulation-ready mode), especially after sudden changes in the regulation signal that induce sudden changes in air flow rate. In addition, large excursions in SAT occur in both cells when the MPC changes the air flow setpoint significantly, for example at hour 08.00. Moreover, the magnitude of SAT oscillations is high at low air flow rates, for example from 05.00 to 08.00.

E. Effect of Fan Control on Chiller Power

The fan and the chiller are thermally coupled through the chilled water loop, hence, it is worth investigating if the chiller's operation is affected while providing frequency regulation with the fan. In Fig. 20 we present relevant experimental results for a duration of 10 hours. The top plot shows the instantaneous and hourly-average electric power of the fan in cell 1A and the chiller. The bottom plot shows the cooling power in the chilled water loop for cells 1A and 1B calculated with (1).

The chiller has two stages and the electric power consumption is relatively constant at each stage. The chiller's cycling depends on cooling load, which in turn depends on fan power and ambient conditions. In general, as the fan power increases the chiller cycles more often and remains longer at the on

This article has been accepted for publication in a future issue of this journal, but has not been fully edited. Content may change prior to final publication. Citation information: DOI 10.1109/TSG.2016.2628893, IEEE Transactions on Smart Grid

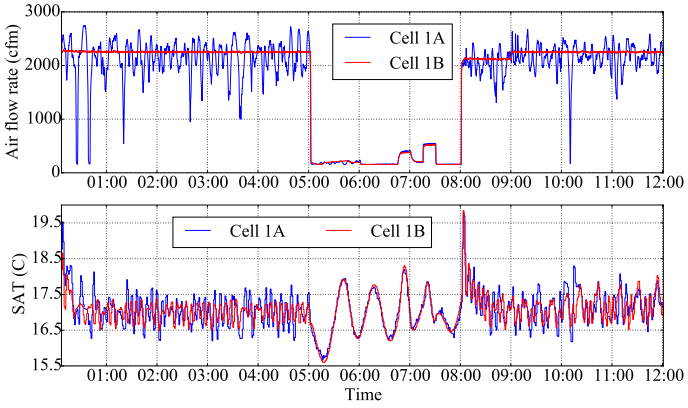

Fig. 19. Air flow rate and SAT in cells 1A and 1B on 20 November.

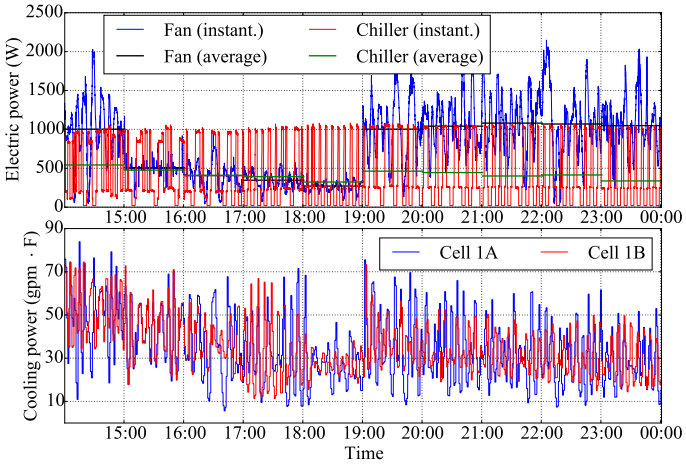

Fig. 20. Effect of frequency regulation on chiller's cycling and cooling power.

state. This can be seen in Fig. 20, where the average chiller power (green line) generally follows the average fan power (black line).

The effect of regulation is visible on cooling power, which fluctuates more in cell 1A compared with cell 1B (regulation-ready mode). Whenever the fan power increases, the cooling load also increases and the SAT tends to decrease. This is sensed by the SAT controller that opens the cooling valve to compensate for the SAT decrease, which in turn increases the cooling power in the chilled water loop. The delay in cooling power response depends on the time constant of the cooling valve's controller.

Despite the oscillations in cooling power, there is no observable effect on chiller's cycling and electric power. This happens because: (i) the chilled water is stored in a tank that provides some inertia; and (ii) the RegD signal is approximately zero-mean. Note that the gradual reduction in the hourly-average chiller electric power from 19.00 to 00.00 in Fig. 20 is mainly the result of a lower cooling need due to ambient temperature drop, rather than a side-effect of frequency regulation.

These results indicate that frequency regulation can be provided with fan control without side-effects on chiller consumption. However, this does not necessarily hold for

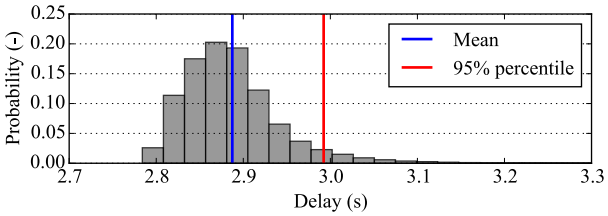

Fig. 21. Histogram of communication delays during the experiment.

regulation signals with a larger energy content such as RegA. In addition, chillers with continuous control (instead of duty-cycle control) will likely display a more observable impact on power consumption while providing frequency regulation, especially if there is no chilled water storage tank. In these cases, the level 3 controller should be revised, which is an interesting direction for future work.

F. Analysis of Communication Delays

A challenge in this experiment was communication delays in measurements and actuation, which result in the overshoots and undershoots in fan power in Fig. 17. In Fig. 21 we present a histogram of the experienced delays during the whole experiment. The probability distribution of delays is positively skewed with a mean value of 2.89 seconds and a 95%-percentile of 2.99 seconds. In fact, there exist a few very large delays in excess of 5 seconds due to temporary unresponsiveness of the CWS, which are not included in Fig. 21. Despite the fact that the average delay is large compared with the time step of level 3 controller (4 seconds), the tracking performance of RegD signal is very good.

VI. Lessons Learned and Outlook

A. Lessons Learned

Hierarchical control is an efficient way to provide frequency regulation with commercial buildings because time-separated tasks are considered individually. Three control layers are essential: (i) a reserve capacity scheduler, (ii) a building climate controller to satisfy comfort while leaving enough slack for reserves, and (iii) a controller to track the regulation signal.

Frequency regulation accuracy: High-quality frequency regulation can be provided by fan speed control. The RegD signal tracking is excellent even with large communication delays in the building automation system. A switched controller comprised of a feedforward controller and a PI feedback controller with gain scheduling provides a fast response without compromising stability. This results in a total PJM score as high as 0.98, which is well above PJM's limit of 0.75.

Means to increase reserve capacity: In our experiment, the fan provided $0.74 - 49.66\%$ of its rated power as reserve capacity, depending on ambient conditions and reserve assumptions. Allowing asymmetric reserve capacities and using a night setback are effective ways to increase the reserve potential from commercial buildings. In fact, down-reserves are preferable for buildings because the capacity can be offered without increasing baseline energy consumption.

Occupant comfort: If the building bids in day-ahead AS markets, respecting occupant comfort might be challenging if the building model and weather forecasts are not very accurate. Furthermore, asymmetric reserves result in a more aggressive scheduling that might increase comfort zone violations.

Building model: An accurate building thermal model is essential for comfort satisfaction, especially in day-ahead AS markets, and periodic calibration of the model helps to account for seasonality and eliminate offsets in modeling error. In general, obtaining accurate day-ahead model predictions is challenging for large commercial buildings, mainly due to uncertainties in occupancy and internal gains [9]. Nevertheless, with an online update of the internal gains, the model's prediction can become fairly accurate for at least one hour ahead. Therefore, offering reserves in an hour-ahead (instead of day-ahead) AS market might be essential for large commercial buildings. Furthermore, large buildings will likely require higher-order thermal models. In order to simplify reserve scheduling and reduce computation time, the building zones can be grouped into a smaller number of groups depending on building geometry [9].

Advantages of MPC: Perhaps the most important advantage of MPC is that it identifies the optimal balance between reserve provision and energy efficiency. MPC additionally provides us with a baseline consumption ahead of real-time operation, which is beneficial from a practical point of view. Moreover, due to its predictive closed-loop nature it reacts to modeling and weather forecast errors in a way that minimizes occupant discomfort.

Robustness measures: It is important to consider the regulation signal uncertainty when scheduling the reserve capacity. A conservative modeling of this uncertainty builds robustness to weather forecast and building modeling errors. Additional robustness can be obtained by tightening the comfort zone constraints in the MPC, and allowing a larger fan speed control band in the MPC compared with the reserve scheduler.

Effects of frequency regulation on building control: Frequency regulation might introduce oscillations in SAT, which can be reduced by appropriately tuning the cooling valve controller. In addition, if the MPC schedules the fan speed at very high values, the cooling loop might not be able to reject the additional heat gain due to fan rotation. On the positive side, there is little effect on the average energy consumption of the chiller while tracking an energy-constrained frequency regulation signal by controlling the fan power. However, the impact of fan control on chiller cycling may prevent the building from accurately following the regulation signal when measured against a baseline that includes the combined consumption of the fan and the chiller. This is an interesting area of further study.

Energy consumption: Provision of frequency reserves entails some energy efficiency loss. The efficiency loss due to scheduling the HVAC consumption in a suboptimal way compared with an energy efficient building control can be as high as 67%. On the other hand, the efficiency loss while tracking frequency regulation signals with limited energy content is negligible.

B. Outlook

There are several avenues for follow-up work. Two direct extensions are to repeat the experiment with the RegA signal of PJM, which is slower but has more energy content, and/or with the heating loop of the AHU enabled. In addition, performing the frequency regulation experiment using all four buildings of FLEXLAB will leverage the full potential of hierarchical control and verify the scalability of the approach.

In some HVAC systems a duct pressure controller regulates the pressure to a fixed setpoint. The combined operation of this controller and the dampers of each zone might reject the frequency regulation action [10]. This is an important challenge that could not be addressed in this experiment at FLEXLAB as it requires testing on a large building.

The reserve scheduling optimization problem might be computationally heavy for buildings with many zones. An alternative is to approximate the nonlinear fan power curve with a piecewise affine function by introducing binary variables. The bilinear building dynamics can be approximated with sequential convex optimization [11], but the convergence is not guaranteed. Finally, the conservativeness of reserve scheduling can be reduced by generating scenarios from historical frequency regulation signals at the cost of reducing robustness.

VII. Conclusion

In Part II of this two-part paper, we reported experimental results for frequency regulation from a commercial building test facility (FLEXLAB). The results are very encouraging: the test building can track fast-moving signals such as RegD reliably, with very high accuracy, and with minimal effect on occupant comfort and the operation of the HVAC system. The results also indicate that a hierarchical control approach is appropriate for frequency regulation with day-ahead bidding of the reserve capacity, and it can be used in field tests and real-world implementations in larger buildings.

Acknowledgements

The work presented in this two-part paper was coordinated by the Consortium for Electric Reliability Technology Solutions (CERTS), and was funded by the U.S. Department of Energy's Office of Electricity Delivery and Energy Reliability under Lawrence Berkeley National Laboratory Contract No. DE-AC02-05CH11231.

We thank Ari Harding, Daniel Fuller, Baptiste Ravache, Rajiv Parmar and Janie Page from LBNL for valuable support and fruitful discussions during the experiment. We acknowledge the help of Michaelangelo Tabone from the University of California, Berkeley, who provided us with Matlab code to predict the clear sky radiation. Finally, we thank David Sturzenegger from Teralytics, Zurich for helpful discussions on building models.

References

[1] E. Vrettos, E. C. Kara, J. MacDonald, G. Andersson, and D. Callaway, "Experimental demonstration of frequency regulation by commercial buildings – Part I: Modeling and hierarchical control design," *IEEE Transactions on Smart Grid (accepted for publication)*.

[2] E. Vrettos, F. Oldewurtel, F. Zhu, and G. Andersson, "Robust provision of frequency reserves by office building aggregations," in *World Congress of the International Federation of Automatic Control (IFAC)*, Cape Town, South Africa, August 2014.
[3] E. Vrettos, F. Oldewurtel, and G. Andersson, "Robust energy-constrained frequency reserves from aggregations of commercial buildings," *IEEE Transactions on Power Systems*, vol. 31, no. 6, pp. 4272–4285, 2016.
[4] B. Givoni, *Passive low energy cooling of buildings*. John Wiley & Sons, 1994.
[5] I. Beil, I. Hiskens, and S. Backhaus, "Round-trip efficiency of fast demand response in a large commercial air conditioner," *Energy and Buildings*, vol. 97, pp. 47–55, 2015.
[6] E. Vrettos and G. Andersson, "Scheduling and provision of secondary frequency reserves by aggregations of commercial buildings," *IEEE Transactions on Sustainable Energy*, vol. 7, no. 2, pp. 850–864, 2016.
[7] "PJM manual 12: Balancing operations," Available online at www.pjm.com/∼/media/documents/manuals/m12.ashx, last accessed 22.02.2016.
[8] Y. Lin, P. Barooah, S. Meyn, and T. Middelkoop, "Experimental evaluation of frequency regulation from commercial building HVAC system," *IEEE Transactions on Smart Grid*, vol. 6, no. 2, pp. 776–783, 2015.
[9] Q. Hu, F. Oldewurtel, M. Balandat, E. Vrettos, D. P. Zhou, and C. J. Tomlin, "Model identification of commercial building HVAC systems during regular operation - empirical results and challenges," in *American Control Conference (ACC)*, Boston, USA, July 2016.
[10] P. Zhao, G. P. Henze, S. Plamp, and V. J. Cushing, "Evaluation of commercial building HVAC systems as frequency regulation providers," *Energy and Buildings*, vol. 67, pp. 225–235, 2013.
[11] F. Oldewurtel, "Stochastic model predictive control for energy efficient building climate control," Ph.D. dissertation, ETH Zürich, 2011.

Evangelos Vrettos (S'09) received the Dipl.-Ing degree in electrical and computer engineering from the National Technical University of Athens (NTUA), Greece, in 2010. After his graduation, he worked as a research assistant at the Electric Machines and Power Electronics Laboratory of NTUA. In 2016 he received the Ph.D. degree from ETH Zürich (Swiss Federal Institute of Technology), Switzerland, where he worked at the Power Systems Laboratory. His research interests include control theory and optimization methods to enable efficient demand response programs for integration of renewable energy sources in the power system. He is also interested in energy storage technologies and energy-efficient control of buildings.

Emre C. Kara (S'12, M'14) is an Associate Staff Scientist at the Grid Integration Systems, and Mobility (GISMo) group at SLAC National Accelerator Laboratory. Prior to that, he was a Postdoctoral Researcher at Lawrence Berkeley National Laboratory (LBNL), Berkeley, CA, USA. He received his Ph.D. degree in civil and environmental engineering from Carnegie Mellon University, Pittsburgh, PA, USA in 2014. His research interests include understanding the energy use of buildings, electric vehicles, modeling, and control of electrical loads to provide demand response services to the grid.

Jason MacDonald (S'14) is a Scientific Research Associate at Lawrence Berkeley National Laboratory, and a Ph.D. student in Energy and Resources at the University of California, Berkeley. He received an MS in Natural Resources and the Environment and an MSE in Mechanical Engineering at the University of Michigan, Ann Arbor in 2011. His research is centered on electricity market participation of distributed energy resources, with particular emphasis in the nexus of market interaction and controls. His work history includes engineering and research in plug-in electric vehicles, photovoltaic systems design, and demand response for ancillary services.

Göran Andersson (M'86, SM'91, F'97) obtained his M.S. (1975) and Ph.D. (1980) degrees from the University of Lund, Sweden. In 1980 he joined ASEA's, now ABB's, HVDC division in Ludvika, Sweden, and in 1986 he was appointed full professor in electric power systems at KTH (Royal Institute of Technology), Stockholm, Sweden. Since 2000 he is full professor in electric power systems at ETH Zürich (Swiss Federal Institute of Technology). His research interests include power system dynamics, control and operation, power markets, and future energy systems. Göran Andersson is Fellow of the Royal Swedish Academy of Sciences, the Royal Swedish Academy of Engineering Sciences, the Swiss Academy of Engineering Sciences, and foreign member of the US National Academy of Engineering. He was the recipient of the 2007 IEEE PES Outstanding Power Educator Award, the 2010 George Montefiore International Award 2010, and the 2016 IEEE PES Prabha S. Kundur Power System Dynamics and Control Award.

Duncan S. Callaway (M'08) is an Associate Professor of Energy and Resources at the University of California, Berkeley. He is also a faculty affiliate in Electrical Engineering and Computer Science, and a faculty scientist at Lawrence Berkeley Laboratory. He received his Ph.D. from Cornell University. He has held engineering positions at Davis Energy Group and PowerLight Corporation, and academic positions at UC Davis, the University of Michigan and UC Berkeley. Duncan teaches courses on electric power systems and energy efficiency in buildings. His research focuses on grid integration of renewable electricity; models and control strategies for demand response, electric vehicles and electricity storage; and energy efficiency in buildings.